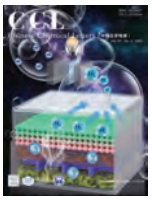
Chinese Chemical Letters 37 (2026) 111567

Contents lists available at ScienceDirect

Chinese Chemical Letters

journal homepage: www.elsevier.com/locate/cclet



Synergistic interaction of ternary Pd–Cu–Ni confined in nanoparticles as pH-universal catalysts for enhanced hydrogen evolution reaction

Xiao Liu[a,1], Haiyan Pang[b,1], Xinrui Kou[b], Zheng Tang[b], Bing Cui[c,*], Shihong Cen[a,*], Yuechang Wei[d,*]

[a] Henan Province Engineering Technology Research Center of Water Environment and Health, College of Pharmacy and Chemical Engineering, Zhengzhou University of Industrial Technology, Zhengzhou 451150, China
[b] Henan Key Laboratory of Polyoxometalate Chemistry, College of Chemistry and Molecular Science, Henan University, Kaifeng 475001, China
[c] Flavors and Fragrance Engineering & Technology Research Center of Henan Province, College of Tobacco Science, Henan Agricultural University, Zhengzhou 450046, China
[d] State Key Laboratory of Heavy Oil Processing, China University of Petroleum, Beijing 102249, China

ARTICLE INFO

Article history:
Received 28 February 2025
Revised 9 May 2025
Accepted 8 July 2025
Available online 9 July 2025

Keywords:
Synergistic effect
pH-universal catalysts
Hydrogen evolution reaction
PdCuNi nanoparticles
Hydrogen economy

ABSTRACT

The development of a high-performance pH-universal electrocatalyst for hydrogen evolution reaction (HER) is a vital step toward hydrogen economy but remains a major challenge. Herein, the Pd, Cu, and Ni three elements were confined in a nanoparticle *via* the microemulsion method. Morphology and structural analysis reveal that PdCuNi nanoparticles are nearly spherical in shape with slight aggregation, and are mainly composed of metallic Pd and Cu, as well as Ni oxide. The electrochemical tests show that PdCuNi exhibits favorable HER catalytic activity in acid (η_{10}: 45 mV; Tafel slopes: 33 mV/dec) and neutral (η_{10}: 71 mV; Tafel slopes: 87 mV/dec) media, and alkaline (η_{10}: 66 mV; Tafel slopes: 116 mV/dec) media. The mechanism analysis implies that the synergistic effect of Pd, Cu, and Ni can improve the inherent conductivity of the catalyst and accelerate the charge transfer process. Furthermore, over 30 h long-term stability has been achieved without significant attenuation. This work provides a strategy for developing versatile and robust multimetallic catalysts towards pH-universal HER.

© 2026 Published by Elsevier B.V. on behalf of Chinese Chemical Society and Institute of Materia Medica, Chinese Academy of Medical Sciences.

Green hydrogen (H_2) energy, a sustainable energy source, is a promising candidate for easing the traditional fossil energy crisis and environmental contamination problems owing to its green products and high specific energy density [1,2]. Green H_2 production through electrochemical water splitting has been considered as one of the most promising approaches for effective conversion and storage of renewable energy [3,4]. In order to lift the conversion efficiency of electricity-to-hydrogen, efficient electrocatalysts with high activity and stability are often applied to reduce the overpotential of hydrogen evolution reaction (HER) [5,6]. In general, the activity of catalysts is closely related to the binding ability with H atoms [7]. At present, platinum (Pt) based catalysts demonstrate excellent HER performance due to their suitable H-binding ability [8]. However, even Pt, which serves as the benchmark catalyst, exhibits significantly lower activity in alkaline media compared to acidic ones [9]. In addition, their high prices and low stability significantly further hinder their widespread application [10]. Theoretically, an ideal electrocatalyst should be capable of operating in a wide pH range [11]. Therefore, it is highly imperative to design Pt-free HER catalysts with Pt-comparable activity in acidic, alkaline, and even the entire pH range. Thereby expanding the application range and improving the overall efficiency of water splitting [12].

To balance activity and cost, other cheaper Pt-group metals such as palladium (Pd) and its derivatives have been attracting more and more attention in the last decade owing to the high catalytic activity for HER [13]. In the past few decades, Pd-based catalysts, such as PdNi nanowires, Pd/NF [14], S-PdNi/C [15], Pd/NiFeO [16], and PdCoNi/C [17] display Pt-like HER activity because of the suitable hydrogen adsorption/desorption energy. Despite good progress having been made, the activity and stability of the reported Pd-based HER electrocatalysts are still far from being desired on account of strong Pd-H bonding hindering the adsorbed H* desorption in catalytic processes [18]. To mitigate this factor, the most common strategy is integrating Pd and some transition metal atoms (such as Ni, Cu, and Co) compositions properly into a single entity, namely multicomponent alloy compounds, which

* Corresponding authors.
E-mail addresses: bingcui@henau.edu.cn (B. Cui), Censhihong2008@163.com (S. Cen), weiyc@cup.edu.cn (Y. Wei).
[1] These authors contributed equally to this work.

https://doi.org/10.1016/j.cclet.2025.111567
1001-8417/© 2026 Published by Elsevier B.V. on behalf of Chinese Chemical Society and Institute of Materia Medica, Chinese Academy of Medical Sciences.

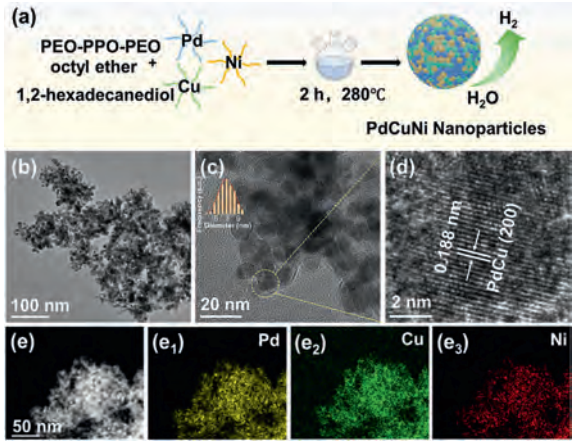


Fig. 1. (a) Schematic illustration of the synthesis of trimetallic PdCuNi nanoparticles. TEM analyses of the PdCuNi nanoparticles: (b) TEM image, (c) magnified TEM image, (d) HR-TEM image, and (e) HAADF-STEM and elemental mapping.

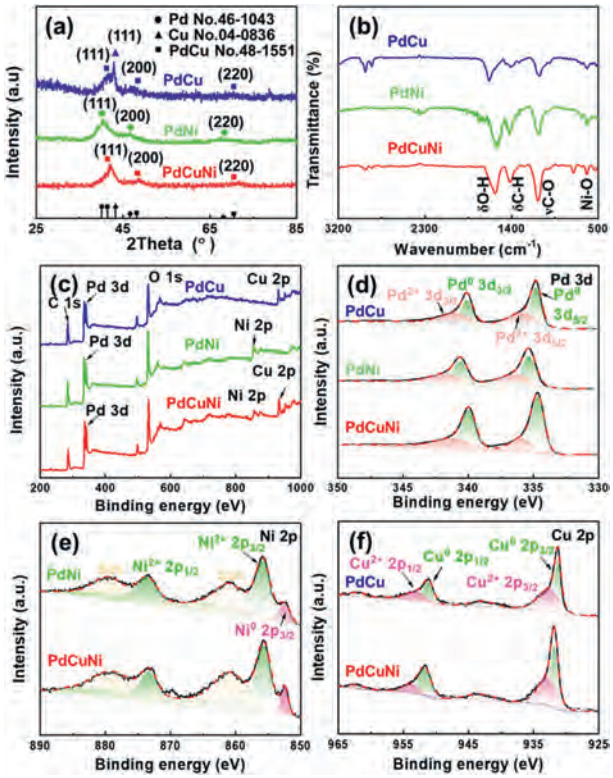


Fig. 2. Structure characterization analyses of the PdCuNi nanoparticles. (a) XRD patterns, (b) Raman spectra. XPS spectra of analyses of the PdCuNi nanoparticles. (c) Full XPS spectra, (d) Pd 3d HR-XPS spectra, (e) Ni 2p HR-XPS spectra, (f) Cu 2p HR-XPS spectra.

could suppress the formation of hydride. More importantly, the introduction of these transition metal atoms not only provides additional active sites and improves the electron transfer rate, but also facilitates the adsorption of the atomic hydrogen produced and its subsequent association to form H_2 from these intermediates owing to the synergic effects between elements [19–22]. In addition, multicomponent alloy compounds also can reduce the material cost for Pd-based electrocatalysts. Although multicomponent alloy compounds possess such advantages, the vast compositional space makes it difficult to design multicomponent catalysts with superior performance. Hence, the rational design and synthesis of Pd-based multicomponent electrocatalysts with high electrocatalytic activity and stability remain critical issues in the construction of high-performance electrochemical energy production systems.

In this work, excellent trimetallic PdCuNi nanoparticles were synthesized *via* a one-pot non-aqueous nanoemulsion process aided by poly(ethylene glycol)-*block*-poly(propylene glycol)-*block*-poly(ethylene glycol) (PEO-PPO-PEO). In the nanoemulsion synthesis, the PEO-PPO-PEO molecules participate in the reactions as a surfactant, besides playing the role of stabilizing the nanoparticles formed, and yet acting as a reducing agent. A series of characterizations (transmission electron microscope (TEM), X-ray photoelectron spectroscopy (XPS), X-ray diffraction (XRD), *etc.*) confirm that Pd, Cu, and Ni elements were integrated into a single entity, and the morphology of PdCuNi nanoparticles is nearly spherical in shape with slight aggregation. Impressively, the obtained PdCuNi nanoparticles as electrocatalyst show outstanding HER performance in all pH electrolytes. The low overpotential for the PdCuNi catalyst is 45, 71, and 66 mV at 10 mA/cm^2 in the acid, neutral, and alkaline electrolyte solution, respectively, which is superior to that of PdCu, PdNi, and CuNi catalysts. Moreover, theoretical analysis reveals that the synergistic interaction of the Pd, Cu, and Ni accelerates charge transfer thereby boosting HER kinetics. This work is supposed to guide designing of efficient multicomponent HER electrocatalysts with high intrinsic catalytic activity.

By utilizing a microemulsion strategy with $Pd(acac)_2$, $Cu(acac)_2$, and $Ni(acac)_2$ as precursors, we successfully prepared PdCuNi nanoparticles in Fig. 1a. Fig. 1b shows the morphology and particle sizes of prepared PdCuNi nanoparticles recorded by TEM. Obviously, PdCuNi nanoparticles are virtually uniform and nearly spherical in shape with slight aggregation. Fig. 1c shows a TEM image of the enlarged area in Fig. 1c more clarity shows a nearly spherical in shape, as well as the corresponding diagrams of the particle size distribution in the inset. The size distribution is reasonably described by the Gaussian function, showing a tight size distribution with average sizes of approximately 6.85 ± 0.04 nm in diameter for PdCuNi nanoparticles. The HR-TEM image of a single PdCuNi hybrid nanoparticle is shown in Fig. 1d. As labeled, the spacing of 1.88 Å indicates the projection of the PdCu (110) plane. To further investigate the elemental composition and distribution, the High-angle annular darkfield-scanning transmission electron microscopy (HAADF-STEM) image of PdCuNi was shown in Fig. 1e. The PdCuNi nanoparticles are composed of Pd, Cu, and Ni elements, while all the elements are distributed homogeneously. The mass ratio of Pd:Cu:Ni is measured to be 1:1:0.7 based on inductively coupled plasma-atomic emission spectrometry (ICP).

The obtained samples were further characterized by XRD and FTIR. Firstly, the crystal structure of the PdCuNi was validated by the X-ray crystal structural analysis in comparison with PdCu and PdNi nanoparticles. As shown in Fig. 2a, for the PdCuNi nanoparticles, the diffraction peaks located at 41.4°, 48.2°, and 70.5° (as symbolized by the square) are allocated to the (111), (200), and (220) crystal planes of PdCu (JCPDS No. 48–1551), demonstrating that metallic PdCu. The same diffraction peaks can be observed in the PdCu nanoparticles. Whereas, different from PdCuNi nanoparticles, PdCu nanoparticles still show an obvious diffraction peak at about 43.3° (as symbolized by the triangle), which can be ascribed to (111) planes of the Cu (JCPDS No. 04–0836). Such a result was further confirmed by TEM (Fig. S1 in Supporting information). In addition, the diffraction peaks of PdNi nanoparticles at 40.1°, 46.6°, and 68.1° (as symbolized by the circle) are appropriately indexed to (111), (200), and (220) planes of the Pd (JCPDS No. 87–0645), respectively. There is no significant Ni diffraction peak in PdNi and PdCuNi samples, which may be ascribed to Ni completely mixed in the Pd lattice [23]. To verify the presence of PEO-PPO-PEO macromolecules, the FTIR spectra of all the samples were analyzed, as shown in Fig. 2b. One sharp bond caused by C–H bend-

ing vibration is shown at ~1413.5 cm^{-1}, then another strong peak appearing in the interval of ~1123.7 cm^{-1} is attributed to C–O–C stretching vibration for three samples [24]. The PdCuNi nanoparticles have a larger BET surface area (24.4 m^2/g) relative to that of PdCu nanoparticles (18.1 m^2/g) and PdNi nanoparticles (17.5 m^2/g), as shown in Fig. S2 (Supporting information).

XPS analysis was performed to investigate the chemical states and compositions of PdCu, PdNi, and PdCuNi nanoparticles. The binding energy in the XPS spectrum was calibrated by C 1s (284.6 eV). The peaks of relevant elements for all samples can be observed from the full-scan XPS spectra (Fig. 2c). The high-resolution Pd 3d spectrum exhibits two doublet peaks, as shown in Fig. 2d. The fitted XPS spectra of the PdCuNi nanoparticles show metallic Pd^0 $3d_{5/2}$ and $3d_{3/2}$ core electron binding energies at 334.6 and 340.0 eV, respectively [25]. In addition, the peaks at 336.0 and 341.2 eV can be indexed as Pd^{2+} [25]. The characteristic peaks of Pd^0 and Pd^{2+} at the same position also can be observed for PdCu nanoparticles. However, it is worth noting that Pd $3d_{5/2}$ and Pd $3d_{5/2}$ doublet peaks appear at higher binding energies (334.8 and 340.1 eV) for PdNi nanoparticles. Such a peak shift is mainly because of electron density from Cu to Pd due to the difference in electronegativity (Pd:2.2; Cu:1.9) [26]. The increased electron density of the Pd causes strong attractive interactions in the inner layer of the Pd atom (3p and 3d orbitals), therefore, the appearance of XPS signals goes to the lower binding energy [27]. Whereafter, the high-resolution Ni 2p spectrum for PdNi and PdCuNi nanoparticles indicates the peaks at 852.5 and 852.4 eV can be indexed as Ni^0, and two other peaks at 873.4 and 873.2 eV can be related to Ni^{2+}, respectively (Fig. 2e) [28]. It is noted that Ni oxides act as supports can modulate the electronic states of metal active sites and optimize the ΔG_{H^*}, which is beneficial to improve activity toward the HER [29]. Apart from the Pd 3p and Ni 3d spectrum, as exhibited in the high-resolution spectrum of Cu 2p for the PdCuNi and PdCu sample (Fig. 2f). Such results reveal the coexistence of Cu^0 and Cu^{2+}. In detail, the major peaks at 931.7 and 931.2 eV are ascribed to Cu^0, and at 932.6 and 932.9 eV are assigned to Cu^{2+} [30]. According to the intensity of the peaks, the Pd^0, Ni^{2+}, and Cu^0 are the most predominant states in PdCuNi nanoparticles.

The electrocatalytic performance of PdCuNi toward HER in an acid media (0.5 mol/L H_2SO_4) by using a standard three-electrode system was evaluated. Firstly, we investigated the effect of Ni and Cu content in the PdCuNi nanoparticles, agglomeration behavior, and size of nanoparticles on catalytic activity, respectively (Figs. S3-S8 in Supporting information). Figs. $3a_1$-a_3 show the linear polarization curves (LSV) of PdCuNi, PdCu, PdNi, and CuNi catalysts at a scan rate of 2 mV/s. As expected, the PdCuNi displays the lowest onset potential, suggesting the synergistic effect between Pd, Cu, and Ni elements. In detail, the overpotentials of PdCuNi require 45 mV to achieve current densities of 10 mA/cm^2 (η_{10}), while overpotentials at 10 mA/cm^2 of the PdCu, PdNi, and CuNi catalysts are 86, 82, and 452 mV, respectively (Fig. $3a_1$). Moreover, the overpotentials at 100 mA/cm^2 (η_{100}) of the PdCuNi catalyst is only 155 mV for HER, which is also much lower than that of PdCu (367 mV), PdNi (252 mV), and CuNi (743 mV), respectively. Tafel slopes were also executed from LSV to assess the catalyst HER kinetics and the relevant reaction mechanism. As is displayed in Fig. $3a_2$, the PdCuNi catalyst also executes the best Tafel slope (33 mV/dec), smaller than PdCu (113 mV/dec), PdNi (86 mV/dec), and CuNi (235 mV/dec). These Tafel slope results match very well with the LSV curves. The smallest Tafel slope of the PdCuNi catalyst manifests the most efficient HER kinetics among all catalysts. The values of these Tafel slopes reveal that the HER rate-determining step abides by the equation: $H_3O^+ + e^- = H_{ads} + H_2O$, and belongs to the Volmer-Heyrovský mechanism [31]. Hence, among all catalysts, the PdCuNi catalyst shows the best HER catalytic activity.

It is well known that electrocatalytic durability is also another important criterion to measure the performance of catalysts. The durability of the PdCuNi nanoparticles was verified *via* chronopotentiometry tests and constant-current technique. Firstly, the chronoamperometric measurement is carried out by loading the catalyst on a glassy carbon electrode (Fig. S9 in Supporting information). After over 30 h of continuous testing, the current-time (*i-t*) curve of PdCuNi catalyst shows good stability, and there was no significant drop in the overall current trend. Whereafter, continuous CV cycles are conducted to show that the LSV curve of the PdCuNi catalyst recorded after 1000 cycles shows a little decreasing overpotential to reach 10 mA/cm^2 compared to the initial curve. In addition, TEM, XPS, and XRD of the PdCuNi catalyst after the stability test in an acidic media have also presented identical structures with the initial electrocatalyst (Figs. S10-S12 in Supporting information). Such results substantiate that the PdCuNi catalyst is highly stable during the long-term HER process. At the same time, the superior HER performance of PdCuNi surpassed those of similar Pd-based catalysts in recently reported literature in Table S1 (Supporting information).

Given some electrolytic cells need to operate in different environments, an effective electrocatalyst is expected to work well in a broad range of conditions, including alkaline and neutral environments. For example, water/chlor-alkali electrolyzers demand an efficient and stable electrocatalyst that can run in an alkaline media [32], whereas microbial electrolytic cells are typically operated in a neutral environment [33]. Hence, for desirable electrocatalysts, the HER catalytic performances in wide pH ranges are very attractive. Based on this point, the electrochemical HER measurements of PdCuNi were performed in neutral (1 mol/L phosphate-buffered saline (PBS), pH 6.7) and alkaline (1 mol/L KOH, pH 14) electrolytes to evaluate the electrocatalytic performance, as shown in Figs. $3b_1$-b_3 and $3c_1$-c_3. In neutral media, PdCuNi catalyst displayed outstanding HER activity with an overpotential of 71 and 360 mV at 10 and 100 mA/cm (Figs. $3b_1$ and $3b_2$), respectively, which is lower than PdCu (η_{10}: 115 mV; η_{100}: 669 mV), PdNi (η_{10}: 134 mV; η_{100}: 772 mV), and CuNi (η_{10}: 472 mV; η_{100}: 1040 mV). The results show overpotentials (η_{10}) of the PdCuNi sample in acid, neutral, and alkaline media are close to those of commercial Pt/C (20 wt%) (acid: 29 mV; neutral: 56 mV; alkaline: 30 mV). The Tafel plots have also been obtained from the LSV curves (Fig. $3b_3$), demonstrating a lower value of PdCuNi (87 mV/dec) than PdCu (184 mV/dec), PdNi (189 mV/dec), and CuNi (230 mV/dec), illustrating the fast inherent HER reaction kinetics and charge transfer rate in neutral solution. Afterward, HER catalytic activity under 1 mol/L KOH was also probed (Figs. $3c_1$-c_3). The PdCuNi requires 66 and 302 mV to reach 10 and 100 mA/cm^2, respectively. Similarly, the Tafel slope of PdCuNi (116 mV/dec) is also the smallest in all catalysts (PdCu: 182 mV/dec; PdNi: 235 mV/dec; CuNi: 327 mV/dec), suggesting that the HER pathway on PdCuNi follows the Volmer–Heyrovsky mechanism under neutral and alkaline solutions. The HER performance of PdCuNi (neutral and alkaline solutions) surpassed those of similar Pd-based catalysts in recently reported literature in Tables S2 and S3 (Supporting information). Finally, the above results demonstrate the excellent performance of PdCuNi in a wide pH range.

To gain insights into the outstanding performance of the PdCuNi catalyst for HER in a wide pH range. Firstly, we predicted the process of HER in acid and alkaline media. Theoretically, HER is a typical two-electron transfer reaction occurring at the cathode of water splitting. Based on the Tafel slope of the PdCuNi catalyst, the reaction in acidic media mainly contains two possible steps (Fig. 4a): Firstly, an electron from an external circuit is transferred to the active site to capture a proton from the electrolyte, resulting in an adsorbed hydrogen atom (*H), then *H on the catalyst surface will preferably combine with a proton and an electron to gener-

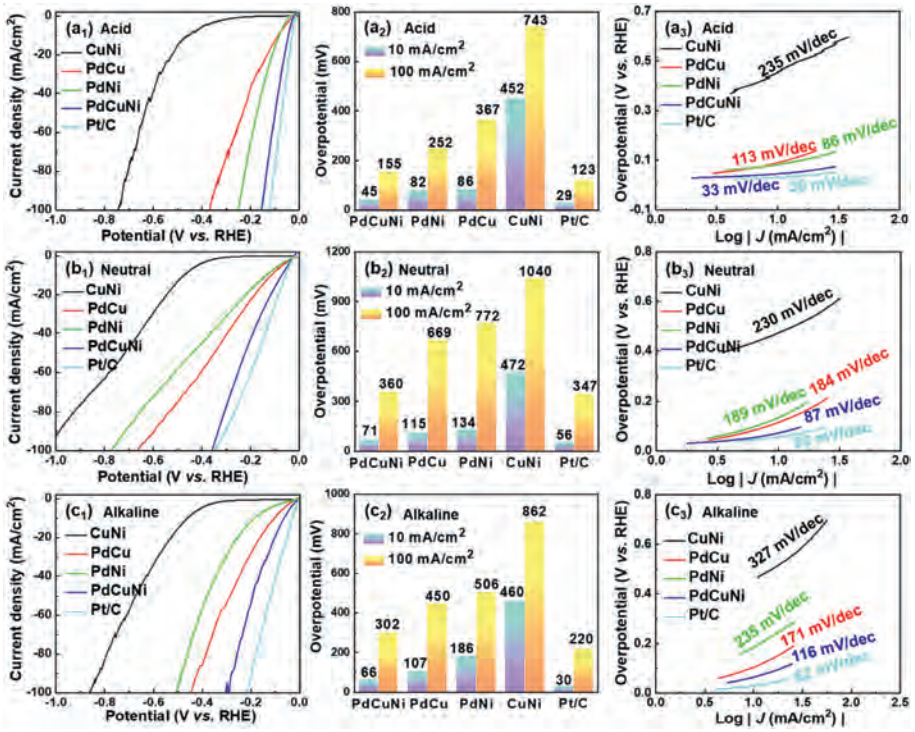


Fig. 3. HER performances of different catalysts (CuNi, PdCu, PdNi, PdCuNi, Pt/C) in acid, neutral and alkaline media. (a_1) LSV curves, (a_2) Overpotential at 10 and 100 mA/cm^2 for HER (a_3) Tafel plots. HER performances of different catalysts (CuNi, PdCu, PdNi, PdCuNi) in a neutral and alkaline media. Neutral media: (b_1) LSV curves, (b_2) Overpotential at 10 and 100 mA/cm^2 for HER, (b_3) Tafel plots. Alkaline media: (c_1) LSV curves, (c_2) Overpotential at 10 and 100 mA/cm^2 for HER, (c_3) Tafel plots.

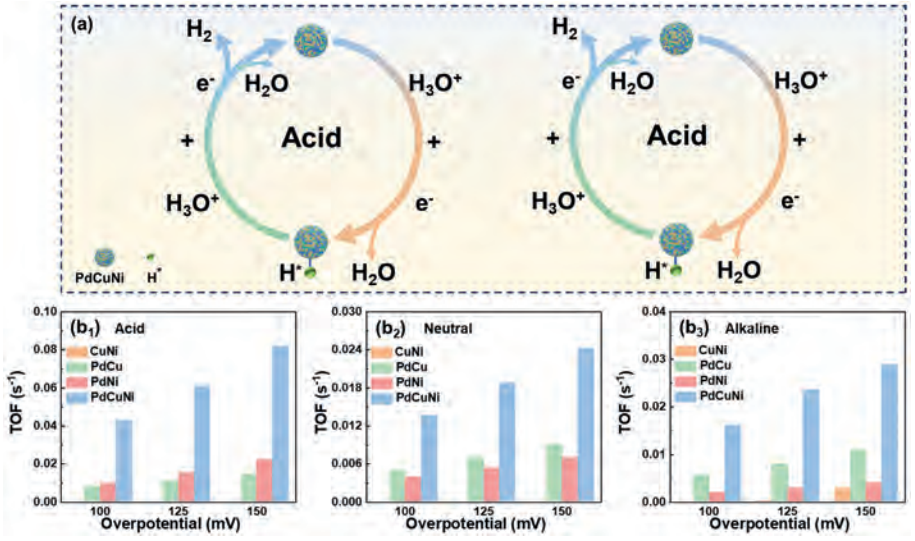


Fig. 4. (a) Schematic of HER mechanism on the PdCuNi nanoparticles in acid and alkaline media. (b) TOF of different catalysts in acid (b_1), neutral (b_2), and alkaline (b_3) media, respectively.

ate H_2 molecules [34]. In the alkaline electrolyte, extra energy is required to dissociate H_2O molecules to obtain enough H^+, which is thermodynamically tougher and leads to higher overpotentials compared to those of acid media. The alkaline HER is first initiated by H_2O adsorption and dissociation process to produce H^* on active sites. Then, H^* will preferably combine with an electron and H_2O molecule to generate an H_2 molecule [35]. The HER mechanism in the neutral electrolyte is nearly identical to that in alkaline environments. It is also possible to acquire a proton from the H_3O^+ in the initial stage due to the existence of the minimal concentration of H_3O^+ ($\sim 10^{-7}$ mol/L). Hence, the HER mechanism in the neutral electrolyte is more complicated, both the reduction of H_3O^+ and H_2O occur in a near-neutral environment, and a detailed process needs to be further understood in the future [36]. Whereafter, the turnover frequencies (TOF) values were calculated to compare the intrinsic catalytic activity of each catalyst [37], as shown in Fig. 4b. As demonstrated in the results, the PdCuNi catalyst demonstrated excellent TOF values in a wide pH range. Specifically, under the overpotential of 100 mV, the TOF values were measured as 0.043, 0.0137, and 0.0289 s^{-1} in 0.5 mol/L H_2SO_4, 1 mol/L PBS, and 1 mol/L KOH, respectively. Notably, PdCuNi nanoparticles exhibited remarkable advantages with the TOF value over that of the PdNi, PdCu, and CuNi catalyst. In addition, the same phenomenon can be observed when the overpotentials are

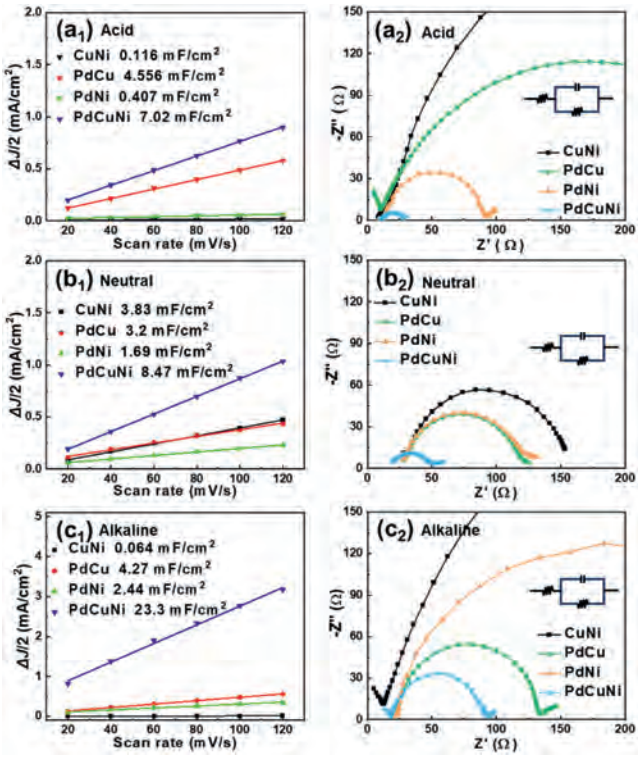


Fig. 5. The linear fit of the capacitive currents of the different catalysts *versus* potential scanning rates from 20 mV/s to 120 mV/s in acid (a_1), neutral (b_1), and alkaline (c_1) media, respectively. Nyquist plots of the electrochemical impedance spectra of different catalysts in acid (a_2), neutral (b_2), and alkaline (c_2) media, respectively.

125 and 150 mV, further supporting the high intrinsic activity of the PdCuNi catalyst in HER.

Subsequently, the electrochemical active surface area (ECSA) and electrochemical impedance spectroscopy (EIS) were evaluated and exhibited to further understand the performance of HER in all pH ranges. The electrochemical double-layer capacitance (C_{dl}) is a reliable criterion for estimating the ECSA (Figs. 5a_1-c_1). C_{dl} was recorded at different scan rates from 20 mV/s to 120 mV/s *via* cyclic voltammetry (Fig. S13-S15 in Supporting information). The calculated C_{dl} are 7.02, 8.47, and 23.33 mF/cm^2 for the PdCuNi catalyst separate in acid, neutral, and alkaline conditions, which is slightly lower than that of PdCu (acid: 4.55 mF/cm^2; neutral: 3.20 mF/cm^2; alkaline: 4.27 mF/cm^2), PdNi (acid: 0.41 mF/cm^2; neutral: 1.69 mF/cm^2; alkaline: 2.44 mF/cm^2), and CuNi (acid: 0.12 mF/cm^2; neutral: 3.83 mF/cm^2; alkaline: 0.06 mF/cm^2). Such results signify that the synergistic effect of the three elements leads to enhanced accessible surface area and plenteous surface-active sites. In addition, to evaluate the charge transfer behaviors, EIS was employed for all samples with the three-electrode system (Figs. 5a_2-c_2). The charge transfer resistance (R_{ct}) values were recorded based on the corresponding Nyquist plots, and the low R_{ct} value indicates high conductivity as well as speedy charge-transfer ability. The R_{ct} values for PdCuNi (acid: 5 Ω; neutral: 11 Ω; alkaline: 33 Ω) are markedly lower than that of PdNi (acid: 34 Ω; neutral: 40 Ω; alkaline: 310 Ω), PdCu (acid: 114 Ω; neutral: 39 Ω; alkaline: 54 Ω), and CuNi (acid: 239 Ω; neutral: 56 Ω; alkaline: 295 Ω) in three electrolytes, attesting the fastest charge-transfer rate of on the PdCuNi surface for HER owing to the synergistic effects between Pd, Cu, and Ni. Accordingly, the enhanced HER performance over the PdCuNi could be attributed to the following reasons: (i) The increased electron density of the Pd can reduce the adsorption energy barrier of H* [38]. (ii) Relatively high content of the metallic Ni improves the inherent conductivity of the catalyst and accelerates the charge-transfer process [39]. (iii) The synergistic effect of Pd, Cu, and Ni is beneficial to providing more accessible active sites [40].

In conclusion, we have successfully prepared trimetallic PdCuNi nanoparticles supported *via* a one-pot non-aqueous nanoemulsion process. The obtained PdCuNi nanoparticles are nearly spherical with an average size of approximately 6.85 nm. At the same time, PdCuNi nanoparticles as catalysts display outstanding catalytic activity for HER with the low η_{10} (45, 71, and 66 mV) and small Tafel slopes (33, 87, and 116 mV/dec) in acid, neutral, and alkaline media, respectively. Additionally, the PdCuNi catalyst also shows excellent HER stability with no significant performance attenuation after successive electrolysis for 30 h in an acid media. Mechanism analysis reveals that the favorable performance of HER is ascribed to higher electron density in the Pd active site and relatively high content of the metallic Ni, which improves the charge transfer efficiency and inherent conductivity of the PdCuNi nanoparticles. This work provides a broad prospect for the development of Pd-based catalysts for application in energy storage and conversion.

Declaration of competing interest

The authors declare that they have no known competing financial interests or personal relationships that could have appeared to influence the work reported in this paper.

CRediT authorship contribution statement

Xiao Liu: Writing – original draft. **Haiyan Pang:** Data curation. **Xinrui Kou:** Data curation. **Zheng Tang:** Data curation, Writing – review & editing. **Bing Cui:** Writing – review & editing. **Shihong Cen:** Writing – review & editing. **Yuechang Wei:** Writing – review & editing.

Acknowledgments

This work was supported in part by the National Natural Science Foundation of China (No. 22406050) and the Natural Science Foundation of Henan Province (Nos. 232300420369, 242300420533).

Supplementary materials

Supplementary material associated with this article can be found, in the online version, at doi:10.1016/j.cclet.2025.111567.

References

[1] Q. Li, Y. Wang, J. Zeng, et al., Chin. Chem. Lett. 32 (2021) 3355–3358.
[2] L. Chen, Y. Wang, X. Zhao, et al., J. Mater. Sci. Technol. 110 (2022) 128–135.
[3] X. Yu, W. Zhang, L. Ma, et al., Green Chem. 27 (2025) 731–742.
[4] J. Li, B. Li, H. Huang, et al., J. Mater. Chem. A 9 (2021) 27061–27071.
[5] Y. Liu, Q. Feng, W. Liu, et al., Nano Energy 81 (2021) 105641.
[6] J.Y. Gao, Y.L. Ma, G.S. Qian, et al., Chem. Commun. 60 (2024) 14224–14227.
[7] Y. Long, Y. Shen, P. Jiang, et al., Sci. Bull. 69 (2024) 763–771.
[8] N. Wu, W. He, S. Shi, et al., J. Colloid Interface Sci. 684 (2025) 658–667.
[9] S. Yang, J.Y. Zhu, X.N. Chen, et al., Appl. Catal. B: Environ. 304 (2022) 120914.
[10] F. Shi, Z. Geng, K. Huang, et al., Adv. Sci. 5 (2018) 1800575.
[11] X.J. Niu, Y.J. Wang, G.H. Gao, et al., J. Colloid Interface Sci. 652 (2023) 989–996.
[12] Y. Pan, K. Sun, S. Liu, et al., J. Am. Chem. Soc. 140 (2018) 2610–2618.
[13] S. Sarkar, S.C.J.I.C.F. Peter, Inorg. Chem. Front. 5 (2018) 2060–2080.
[14] J. Wang, X. Wei, P. Wang, et al., Fuel 341 (2023) 127689.
[15] Ö. Şahin, A. Akdag, S. Horoz, et al., Fuel 346 (2023) 128391.
[16] W. Zhang, X. Jiang, Z. Dong, et al., Adv. Funct. Mater. 31 (2021) 2107181.
[17] Y. Pan, Y. Zhu, J. Shen, et al., Nanoscale 11 (2019) 17334–17339.
[18] X. Yang, W. Xu, S. Cao, et al., Appl. Catal. B: Environ. 246 (2019) 156–165.
[19] S. Wang, B. Xu, W. Huo, et al., Appl. Catal. B: Environ. 313 (2022) 121472.
[20] H. Li, J. Lai, Z. Li, et al., Adv. Funct. Mater. 31 (2021) 2106715.
[21] L. Chen, H. Guo, T. Fujita, et al., Adv. Funct. Mater. 21 (2011) 4364–4370.
[22] X. Cao, Y. Han, C. Gao, et al., Nano Energy 9 (2014) 301–308.
[23] G. Liu, L. Shu, D. Yan, et al., Int. J. Hydrogen Energy 50 (2024) 1146–1156.
[24] P. Yang, X. Liu, Z. Liu, et al., Adv. Funct. Mater. 34 (2024) 2405908.

[25] S. Cai, X. Liu, Q. Han, et al., Nano Res. 11 (2018) 3272–3281.
[26] M.D. Obradović, U.Č. Lačnjevac, V.V. Radmilović, et al., J. Electroanal. Chem. 944 (2023) 117673.
[27] X. Liu, L. Xiao, J. Weng, et al., Sci. Adv. 6 (2020) eabb4359.
[28] S. Zhang, A. Pei, G. Li, et al., Green Chem. 24 (2022) 2438–2450.
[29] J. Wang, S. Mao, Z. Liu, et al., ACS Appl. Mater. 9 (2017) 7139–7147.
[30] S.C. Qi, Y.J. Zhao, X.J. Lu, et al., Chem. Sci. 15 (2024) 7285–7292.
[31] J. Zhang, A. Motta, Y. Gao, et al., ACS Catal. 8 (2018) 4893–4901.
[32] Z. Pu, I.S. Amiinu, Z. Kou, et al., Angew. Chem. Int. Ed. 56 (2017) 11559–11564.
[33] M. Borgolte, O. Riester, I. Quint, et al., Mater. Today Chem. 26 (2022) 101176.
[34] J. Li, J. Zhang, J. Shen, et al., Mater. Chem. Front. 7 (2023) 567–606.
[35] J. Li, J. Zhang, J. Zhang, et al., J. Mater. Chem. A 11 (2023) 19812–19844.
[36] M. Li, X. Wang, J. Meng, et al., Adv. Mater. 36 (2024) 2308628.
[37] T. Zhu, J. Han, T. Sun, et al., ACS Catal. 14 (2024) 1914–1921.
[38] Y. Cao, R. Guo, M. Ma, et al., Acta Phys. Chim. Sin. 40 (2024) 2303029.
[39] X. Peng, X. Jin, N. Liu, et al., Appl. Surf. Sci. 567 (2021) 150779.
[40] Y. Zheng, J. Rong, J. Xu, et al., Appl. Surf. Sci. 563 (2021) 150385.